



HAL
open science

Origin of area selective plasma enhanced chemical vapor deposition of microcrystalline silicon

Ghewa Akiki, Mathieu Frégnaux, Ileana Florea, Pavel Bulkin, Dmitri Daineka, Sergej Filonovich, Muriel Bouttemy, Erik Johnson

► To cite this version:

Ghewa Akiki, Mathieu Frégnaux, Ileana Florea, Pavel Bulkin, Dmitri Daineka, et al.. Origin of area selective plasma enhanced chemical vapor deposition of microcrystalline silicon. *Journal of Vacuum Science & Technology A*, 2021, 39 (1), pp.013201. 10.1116/6.0000653 . hal-03060642

HAL Id: hal-03060642

<https://hal.science/hal-03060642>

Submitted on 14 Dec 2020

HAL is a multi-disciplinary open access archive for the deposit and dissemination of scientific research documents, whether they are published or not. The documents may come from teaching and research institutions in France or abroad, or from public or private research centers.

L'archive ouverte pluridisciplinaire **HAL**, est destinée au dépôt et à la diffusion de documents scientifiques de niveau recherche, publiés ou non, émanant des établissements d'enseignement et de recherche français ou étrangers, des laboratoires publics ou privés.

Origin of Area Selective Plasma Enhanced Chemical Vapor Deposition of Microcrystalline Silicon

Ghewa Akiki,¹ Mathieu Frégnaux,² Ileana Florea,¹ Pavel Bulkin,¹ Dmitri Daineka,¹ Sergej Filonovich,³ Muriel Bouttemy² and Erik V. Johnson^{1,a)}

¹ LPICM-CNRS, Ecole Polytechnique, Institut Polytechnique de Paris, Route de Saclay, 91120 Palaiseau, France

² Institut Lavoisier de Versailles (ILV), Université de Versailles Saint-Quentin en Yvelines, Université Paris-Saclay, CNRS, UMR 8180, 45 avenue des Etats-Unis, 78035 Versailles Cedex, France

³ TOTAL GRP, 2 Place Jean Millier – La Défense 6, 92078 Paris La Défense Cedex, France

^{a)}Electronic mail: ghewa.akiki@polytechnique.edu

Abstract

Plasma Enhanced Chemical Vapor Deposition of silicon from SiF₄/H₂/Ar gas mixture is observed on a SiO_xN_y surface, while under the same plasma conditions, silicon films do not grow on AlO_x nor Al surfaces. Transmission electron microscopy confirms that the silicon deposited on SiO_xN_y has a microcrystalline structure. After the plasma process, fluorine is detected in abundance on the AlO_x surface by X-ray photoelectron spectroscopy and energy dispersive X-ray chemical analyses. This suggests that Al-F bonds are formed on this surface, blocking any deposition of silicon on it. In-situ ellipsometry studies show that deposition can be initiated on AlO_x surfaces by increasing the temperature of the electrodes or increasing the RF plasma power, leading to a loss of selectivity.

I. Introduction

The development of processes that can limit material deposition to one type of surface area without using lithography have recently gained increased attention from the microelectronics industry. Such processes, called area-selective deposition (ASD), are designed to promote deposition on the “growth” area of a substrate while preventing deposition on a “non-growth” area. Atomic Layer Deposition (ALD) and Chemical Vapor Deposition (CVD) are the most widely-used techniques used to achieve ASD, depositing metals, semiconductors, and insulators¹. These techniques work either by activating the growth surface, passivating or deactivating the non-growth area surface, adding a co-reagent to the precursors, or treating the surfaces prior to the process in a way to block any deposition or etching^{2,3}.

In the case of CVD, the selective epitaxial deposition of semiconductors such as silicon and GaAs has been demonstrated using silicon tetrachloride/hydrogen and an undoped GaAs source/ HCl or

AsCl₃/H₂, respectively^{4,5}. In these cases, chlorine is the factor that promotes the selectivity, as it can reduce the rate of deposition of Si and Ga⁶.

As for metals, selective tungsten deposition has been demonstrated by CVD using WF₆/H₂ gases. In this case, bare silicon is considered as a solid reducing agent, as it can lose an electron and dissociate WF₆ to deposit tungsten. Once the first W layer is formed, any gaseous reducing agent such as H₂ or silane reduces WF₆ and assures a steady growth of W. On the other hand, no reduction of WF₆ precursor occurs on SiO₂ surface since Si in SiO₂ is totally oxidized, preventing W growth^{6,7}.

For the selective CVD of metallic aluminum on Si/SiO₂ patterned samples using triisobutylaluminum (TIBA), the reaction of the precursors with SiO₂ surfaces led to a creation of a monolayer of C and Al that doesn't react with additional precursor⁸. Yet, on the non-growth surface, the precursor either does not stick directly or it reacts and saturates the surface with a relatively stable layer blocking the reaction of additional precursor coming on it⁹.

Moreover, area selective deposition by CVD can be enhanced by adding an inhibitor to the process that passivates one surface and promotes deposition on another. as it is the case for MoC_xN_y, Fe and Ru thin films deposited selectively on metal surfaces vs oxide surfaces¹⁰ or the selective deposition of Co thin film on acidic oxides versus basic oxides when a NH₃ flow is added to the precursors¹¹. Another AS-CVD approach is to introduce a 4-octyne "co-adsorbate" species during the process. Those species bind strongly to Cu surfaces compared to SiO₂ surfaces blocking the growth of ZrO₂ film on Cu¹².

For AS-ALD, the passivation of the non-growth surface results from a pretreatment prior to the film deposition process. This can be done either by using organic films such as self-assembled monolayers (SAMs)¹³⁻¹⁶ or polymers¹⁷ that preferentially react with a certain type of surfaces (metal or oxides) inhibiting any film growth, or by exposing the surface to an H₂ plasma¹⁸. However, many constraints face this methodology, such as the adsorption of the precursor on the inhibitor, or losing the inhibitor molecules after few cycles¹⁹. Current ASD research focuses on alternating deposition and etching to get the desired selective deposition. The resulting supercycle method benefits from the nucleation delay between two different surfaces to obtain the first selective film deposited and then introduce the etch step to reinitiate a new nucleation delay^{20,21}.

In this work, we explore the use of a low temperature variant of CVD, namely Plasma-Enhanced Chemical Vapour Deposition (PECVD) to achieve ASD. In recent work, area selective PECVD has been demonstrated on SiN_x versus AlO_x surfaces by using an Ar/SiF₄/H₂ gas mixture²². In this paper we use the same plasma chemistry, and aim to identify the underlying causes (physical or chemical) behind the area selective PECVD of microcrystalline silicon films on SiO_xN_y vs AlO_x.

II. Experimental Description

A. Sample preparation

AlO_x was deposited on silicon substrates by Atomic Layer Deposition (ALD) using trimethylaluminum (TMA) and water as precursors (500 ALD cycles). A part of the the AlO_x coated Silicon wafer was then masked by a piece of scrap silicon, and a SiO_xN_y layer was deposited using an Electron Cyclotron Resonance (ECR-) PECVD system. The resulting sample is represented schematically in figure 1.

B. Ar/SiF₄/H₂ PECVD

The area-selective deposition of $\mu\text{c-Si:H}$ thin films was performed in the ATOS PECVD reactor. ATOS is a Radio Frequency-Capacitively Coupled Plasma (RF-CCP) system with a load lock, and which is equipped with an in-situ ellipsometer (J.A Woollam RC2). Spectra were measured for the range from 1.3 eV - 5 eV and modelled using the Tauc-Lorentz dispersion formula. The inter-electrode distance is 25 mm and the working pressure is 1.7 Torr. Each electrode is heated independently but were both set to identical temperatures for all experiments. The Ar/SiF₄/H₂ flow rates used were 200/20/14 sccm. For some samples, an a-Si:H “capping” layer was deposited after the selective deposition process for XPS studies (see fig.1).

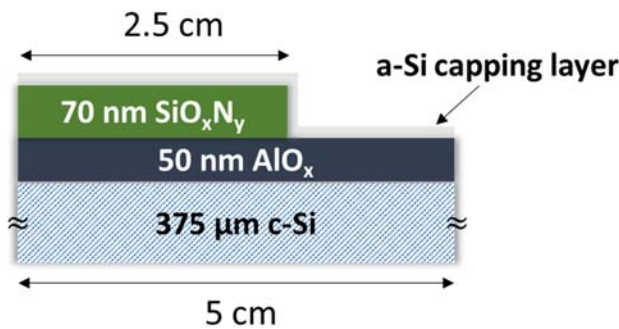


FIG. 1. Schematic representation of sample substrates. The amorphous silicon (a-Si) capping layer is 10 nm thick.

C. TEM and EDX sample preparation

Transmission Electron Microscopy (TEM) and Energy Dispersive X-Ray (EDX) analysis were performed on a Titan Themis transmission electron microscope operating at 200 kV equipped with a Cs aberration probe corrector and a Super X that allows chemical analyses of light and heavy elements with a spatial resolution in the nm range. For this, cross-sectional sample lamellas have been prepared using a standard lift-out procedure in a Focused Ion Beam dual beam microscope (FIB, FEI-Scios Dual Beam). For the chemical analyses by EDX, we have chosen the following as elements of interest: silicon (with an ionization edge at $K\alpha=1.74$ KeV), oxygen ($K\alpha=0.523$ KeV), aluminum ($K\alpha=1.48$ KeV), fluorine ($K\alpha=0.67$ KeV) and nitrogen ($K\alpha=0.39$ KeV). Carbon and platinum protective layers have been deposited on top of the sample prior to the FIB milling process in order to prevent Ga ion implantation during the milling process.

XPS analysis (surface and profiling)

X-ray Photoelectron Spectroscopy (XPS) measurements were carried out at Institut Lavoisier Versailles on a Thermofisher Scientific NEXSA spectrometer equipped with a monochromated Al-K α anode (1486.6 eV) and a dual flood gun (low energy electron and ion). Despite the use of charge compensation, a differential charging effect could not be avoided. Consequently, the spectra are presented without any specific energy scale recalibration, and should therefore be interpreted comparatively. High energy resolution spectral windows of interest were recorded with a 400 μm spot size. The photoelectron detection was performed using a constant analyzer energy (CAE) mode (20 eV pass energy) and a 0.1 eV energy step.

XPS depth profiling required the use of the Thermofisher Scientific MAGCIS dual-beam ion gun. Monoatomic argon (Ar⁺) ions were accelerated to reach the sample with a kinetic energy of 2000 eV and an angle of 30° from the surface normal. The thin films were irradiated on a square area of 2×2 mm².

Quantification was performed based on the Al2p, Si2p, C1s, N1s, O1s, F1s photopeak areas after a Shirley type background subtraction using the Thermofisher Scientific Advantage© software and its “ALTHERM01” library as sensitivity factor collection. A Gaussian-Lorentzian convolved function with L/G =30% was used for the XPS Al2p spectra reconstruction. The spin-orbit coupling Al2p_{1/2}-Al2p_{3/2} was set to 0.44 eV.

III. Selectivity Process Window

A. Selective deposition process for Ar/SiF₄/H₂ PECVD

Through many trials, a process window for selective deposition was determined. Reliable selectivity is obtained when a process condition consisting of 8W RF power and a substrate/electrode temperature of 100 °C were used, a gas flow mixture of Ar/SiF₄/H₂ = 200/20/14 sccm and a total pressure of 1.7 Torr. The results shown in this section are for such plasma conditions.

During the plasma process, deposition was monitored by in-situ ellipsometry; ellipsometric spectra were acquired once every second and were fitted using the CompleteEASE software in the following way: the underlying substrate layers were first measured and modelled prior to plasma ignition, and then left unchanged during the subsequent modelling during growth. The deposited silicon layer is modeled using a Tauc Lorentz (TL) dispersion function and a surface roughness, represented by a mixture of 50% of $\mu\text{c-Si}$ with 50% of void using Bruggeman Effective Medium Approximation. The TL optical constants were chosen to fit with the thickest layer, present at the end of deposition. Then, the thicknesses of the parameterized layer (as well as the surface roughness) were fitted starting from the end-point, then progressing backwards in time, allowing only the thickness of the layer to change.

For the same plasma conditions, in-situ ellipsometric spectra of different surfaces were measured in separate runs (with final spectra confirmed ex-situ). Figure 2 shows the thickness of deposited silicon with time on SiO_xN_y, AlO_x, and aluminum surfaces. Aluminum surfaces were prepared by

coating a 50 nm layer of aluminum on a silicon substrate using thermal evaporator. Silicon growth only occurs on the SiO_xN_y layer, while no deposition occurred on the AlO_x or Al surfaces. As a result, a 55 nm thick silicon film is deposited selectively on SiO_xN_y area versus AlO_x area (see sample in fig.1). Moreover, the optical constants of the silicon layer as well as the shape of the roughness evolution is consistent with microcrystalline silicon growing on top of SiO_xN_y ^{23,24}. It should also be mentioned that the Mean Squared Error (MSE) between measured data and model-generated data is maximal in the beginning of the process then it decreases with time as the layer becomes denser and less rough.

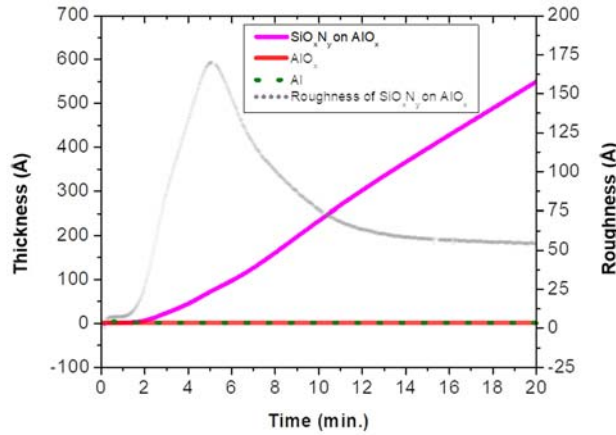


FIG. 2. Silicon layer thickness and surface roughness with time measured by in-situ ellipsometry on SiO_xN_y , AlO_x and Al surfaces.

B. Non-selective deposition process for Ar/SiF₄/H₂ PECVD

Performing a plasma process outside of the selectivity process window (mentioned in the previous section) results in selectivity breakdown, manifested as silicon growth on an AlO_x surface. Specifically, deposition occurs on an AlO_x surface when increasing the RF power (from 8W to 15W) or the temperature of the electrodes (from 100°C to 175°C). In the example presented below, Ar/H₂/SiF₄ gas flows and pressure are set the same as in the previous experiment, 200/20/14 sccm and 1.7 Torr respectively. Selectivity is lost for 15 Watts/100°C and for 10 W/175°C, as shown in figure 3. Furthermore, it is clear that deposition on the AlO_x area evolves very differently than on SiO_xN_y , as the roughness and thickness display very distinct, abrupt changes and non-monotonicity, respectively. It should also be noted that using conditions between 8 and 15 W and between 100°C and 175°C results in unpredictable selectivity, which depends on factors including wall conditions, substrate storage time before processing, and even substrate type (AlO_x films on glass will not allow growth, but films on c-Si will).

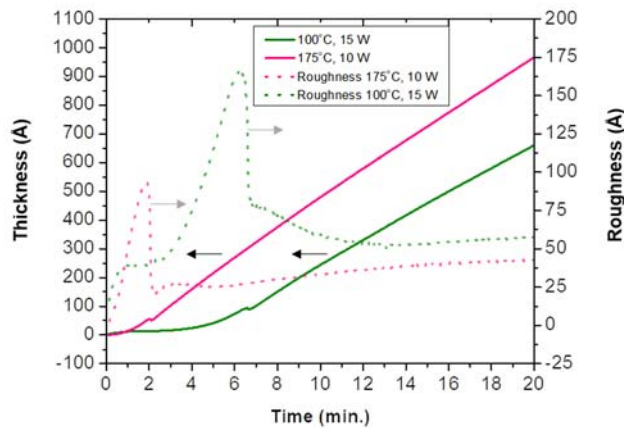


FIG. 3. Microcrystalline silicon ($\mu\text{c-Si:H}$) film thickness with time deposited on Aluminum Oxide (AlO_x) for a power of 15 W (green curve) and a temperature of electrodes of 175°C (pink curve).

IV. Physical Origin of Selectivity

A. TEM Measurements

Structural and chemical characterizations at high resolution were performed using the TEM and Scanning TEM High-Angle Annular Dark Field (STEM-HAADF) imaging mode near the surfaces of two representative samples containing the SiO_xN_y and AlO_x layer.

A STEM-HAADF image on the cross sectional lamella containing first only the AlO_x area is presented in figure 4. As it can be observed, even though the sample was exposed to the PECVD process using the SiF_4 precursor, no trace of any Si layer was observed near the surface (there is only the protective layer, which is a carbon layer deposited prior to the FIB fabrication of the lamella). Another typical finding that can be observed from the HAADF-STEM EDX mapping involves the presence of fluorine, in very small amount, detected primarily on the surface of the AlO_x layer. It is likely that those F atoms are bonded to Al atoms because otherwise fluorine is expected to be difficult to detect once the surface is exposed to the atmosphere for any length of time.

Regarding the second sample, for which a SiO_xN_y area was exposed to the plasma process, a TEM image of its corresponding cross-sectional lamella clearly shows the multi-layer stack (figure 5). A closer analysis by Fast Fourier Transform (FFT) on the silicon layer deposited on top of SiO_xN_y brings into evidence its microcrystalline structure (as was expected from SE analysis) with crystallite dimensions of few nanometers. Concerning the fluorine presence from the STEM-HAADF EDX chemical analysis, one can notice it is present mostly inside the SiO_xN_y layer (unlike the AlO_x layer, where F was only present at the surface). This must result from the diffusion of F atoms into this layer during the deposition of $\mu\text{c-Si:H}$ (using a SiF_4 plasma precursor), as no F is present in the precursors for SiO_xN_y growth. One can also note the absence of F in the silicon substrate in both cases.

In order to understand the structure of the SiO_xN_y layer, a capping layer of AlO_x was deposited by ALD, and then the sample was prepared as a lamella, as previously described. Figure 6 shows that the SiO_xN_y layer indeed has a columnar structure that most likely allows the in-diffusion of F during deposition of a layer on top.

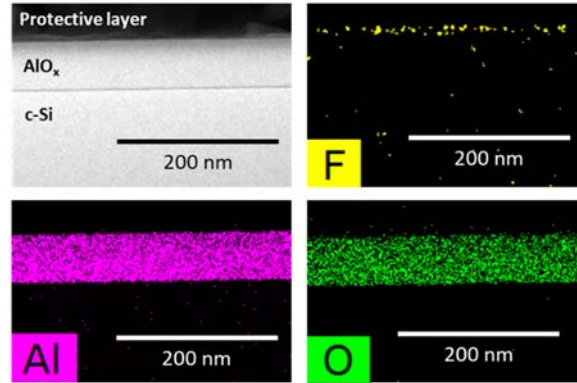


FIG. 4. HAADF image with its corresponding STEM-EDX chemical mapping of AlO_x area with the chosen element of interest F (yellow), Al (pink), and O (green)

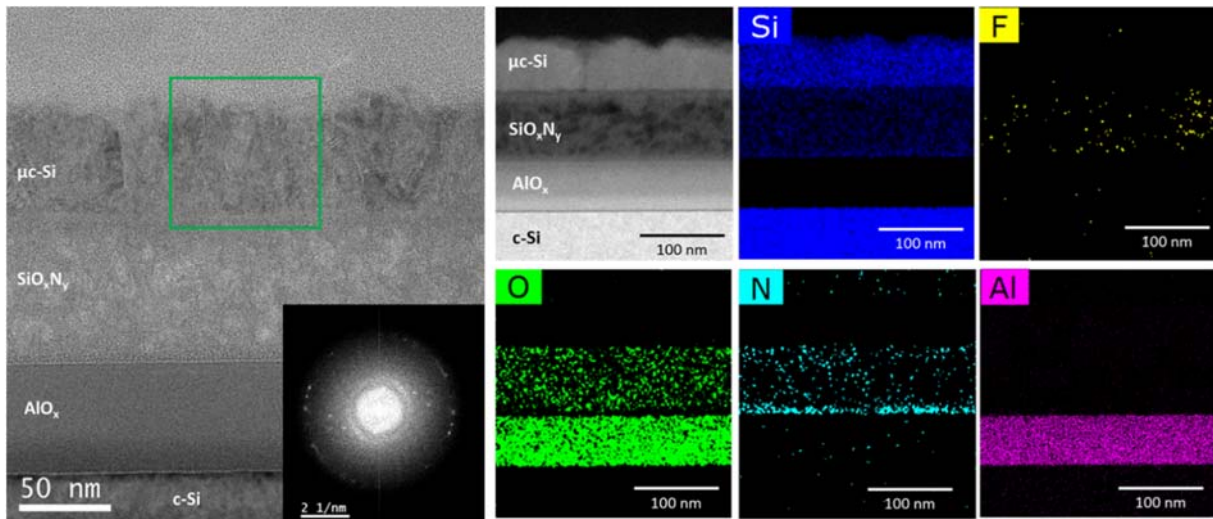


FIG. 5. Bright Field TEM, STEM and EDX chemical analysis of SiO_xN_y area. The inset on the right edge of the TEM image is the FFT profile that confirms the microcrystalline structure of the top layer

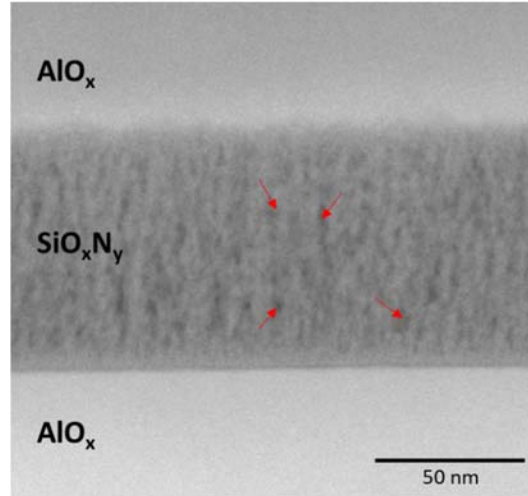


FIG. 6. STEM-HAADF image of $\text{AlO}_x/\text{SiO}_x\text{N}_y/\text{AlO}_x$ showing the columnar growth of SiO_xN_y layer

B. XPS Measurements and Analysis

The SiO_xN_y and AlO_x surface chemistries resulting from the selective deposition process with $\text{Ar}/\text{SiF}_4/\text{H}_2$ plasma (described in the experimental section) have been investigated using X-ray Photoelectron Spectroscopy (XPS). In order to preserve the integrity of the chemical information and minimize surface contamination, an encapsulation layer consisting of 10 nm of amorphous silicon layer was deposited on top, using a SiH_4/H_2 plasma. The chemical composition at the buried interfaces was determined by sequential depth profiling of each stack, and the corresponding in-depth overall atomic percentage profiles are presented in Figure 7. For both SiO_xN_y and AlO_x areas, C and O are present at the initial, extreme surface and correspond to the adventitious carbon layer inherent to ambient air exposure. No trace of fluorine is observed within the $\mu\text{c-Si:H}$ layer. This means that the F from the SiF_4 precursor is fully scavenged by H during the growth process, at least to a level below the XPS detection threshold. This result is consistent with previous studies^{25,26}. All the different interfaces are sharp and clearly identified. Concerning the SiO_xN_y area, the $\mu\text{c-Si:H} / \text{SiO}_x\text{N}_y$ interface is reached after 370 s sputtering. During the profiling of this SiO_xN_y layer the O and Si contents are roughly constant although a F gradient (12 at.% maximum value) is visible, negatively correlated to the N distribution. This confirms the trend evidenced by the STEM-EDX analysis, also showing F incorporation. For the AlO_x area, F is only localized at the a-Si/ AlO_x interface and reaching a content of 18 at%.

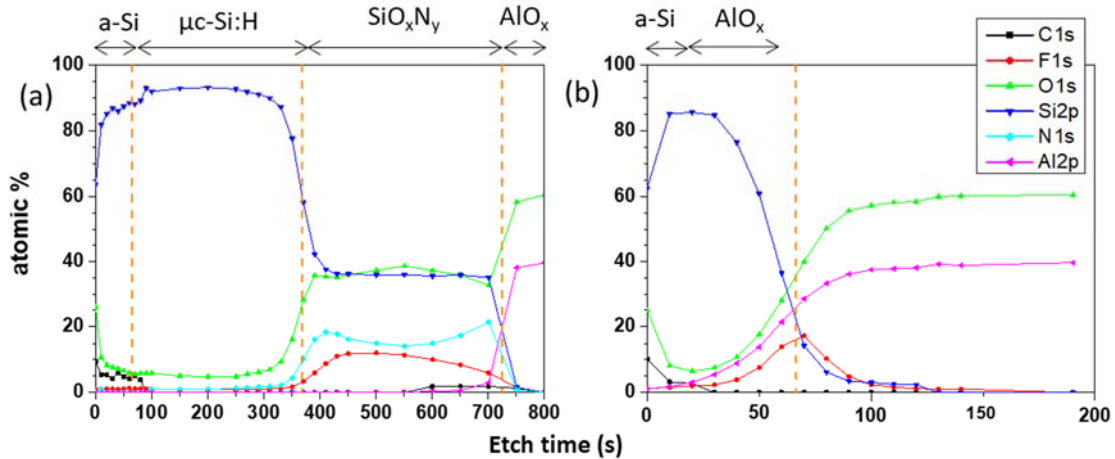


FIG. 7. XPS depth profiles of **(a)** SiO_xN_y and **(b)** AlO_x areas on c-Si substrate. (Note: x axis scales are not the same for both graphs).

In addition to these elemental chemical composition profiles, a fine XPS analysis was conducted using high-energy-resolution spectral windows in order to access information on the chemical environments of each element. We will focus on the AlO_x area where no deposition occurs. The evolution of the Al2p peak during profiling is shown Figure 8 (a). Note that the a-Si layer is very thin (less than the escape depth of Al2p photoelectrons), so the Al is detected even before sputtering. The Al2p peak position is progressively shifted toward lower binding energies with increase sputtering time, i.e. when probing the bulk AlO_x layer. This behavior is consistent with the presence of a more electronegative element at the surface compared to the bulk and clearly suggests the formation of Al-F bonds at the surface of the AlO_x layer. Indeed, a fit of the Al2p photopeak representative of the AlO_x surface (70 s etching time on the profile of Figure 7 (b)) is presented in Figure 8 (b), and requires two doublets, attributed to Al-O and Al-F bonds, whose energy positions are shifted by 1.5 eV. The expected energy difference is around 2.0 eV for pure Al₂O₃ and AlF₃ compounds²⁷ suggesting a rather mixed Al-O-F environment at the surface of the AlO_x layer. An Al-O/Al-F ratio of 2.66 is estimated, leading to a ratio of F/Al=2.9. This indicates that the amount of F exceeds the number of Al sites available, so in fact only a part of the F is really bonded, and the rest is likely adsorbed on top.

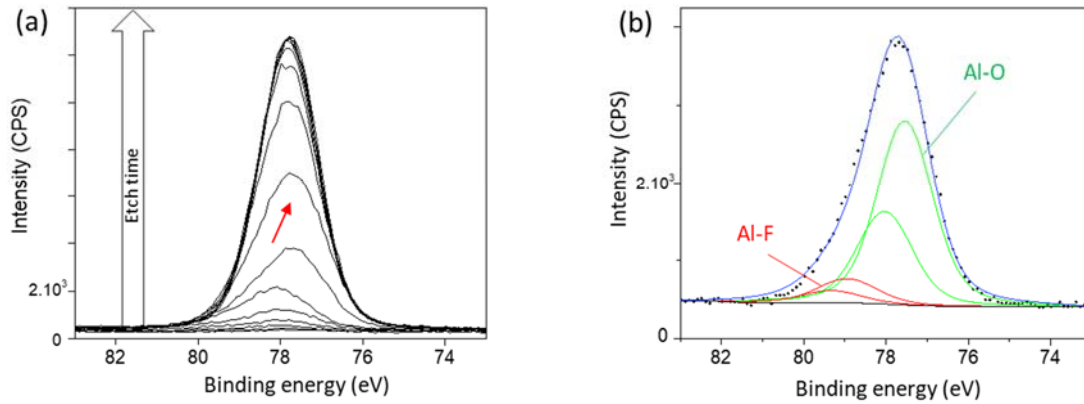


FIG. 8. (a) Al₂p photopeak evolution with etching time for a-Si/AlO_x/c-Si sample and (b) typical Al₂p fit at the AlO_x surface, *i.e.* 70 s etching time.

The same analyses have been carried out on two other samples: one before any plasma process (as a reference, labelled “Ref AlO_x”) and another with a selective deposition process but without any capping layer (labelled “w/o a-Si cap”). Figure 9 shows the Al₂p photopeaks for those three samples. It is clear that after exposure to the Ar/SiF₄/H₂ plasma, a new contribution at high binding energy, attributed to Al-F bonds, is detected. It is also interesting to note that according to Al-O/Al-F atomic percentage ratio, the amount of Al-F bonds is higher on the sample with the a-Si capping (Al-O/Al-F=3.21) compared to the one without (Al-O/Al-F=5.44). This indicates that some of the Al-F bonds created during the selective deposition process are removed from the AlO_x surface to allow the deposition of the a-Si:H film. It can be concluded that the more Al-F bonds that are present, the better selectivity is obtained, which is also consistent with lack of deposition on metallic Al presented in figure 2.

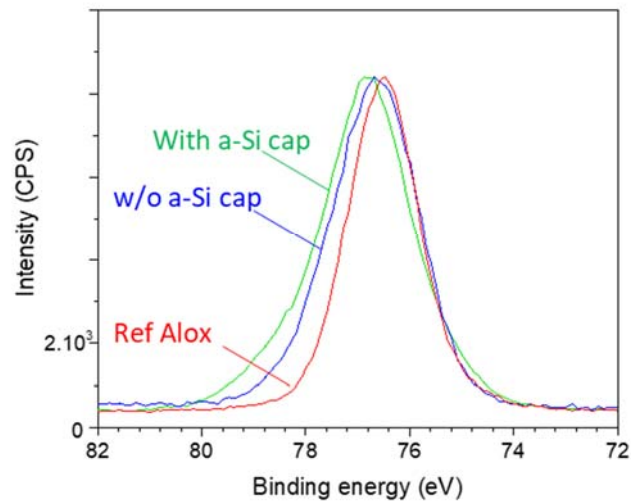


FIG. 9. Comparison of Al2p photopeaks of AlO_x area before plasma process (red) and after (green with a-Si capping layer, and blue without).

V. CONCLUSIONS

In this work, we have attempted to identify the origins of area selective deposition of silicon by PECVD when comparing SiO_xN_y and AlO_x surfaces. The TEM and XPS analyses show a very high density of Al-F bonds at the surface of the non-deposition, AlO_x surface. It can be concluded that Al-F bonds block the deposition of Si, as they form a “chemical” mask that provides selectivity. However, process windows studies show that increased temperature or increased power both weaken this blocking layer. SiO_xN_y does not display the presence of this blocking layer. For the samples in this study, F is incorporated inside the SiO_xN_y layer due to its columnar structure, however, this incorporation is not sufficient to prevent the growth of silicon on these surface areas. The model of Al-F bonds preventing the growth of Si is also consistent with the demonstrated non-growth on an Al surface. The metric of strong F bonds with a growth surface may also provide a good prediction mechanism for whether surfaces will be selective to Si growth or not.

In addition, when selectivity breaks down outside of the process window and growth occurs on an AlO_x surface, the in-situ SE displays unusual features. The plot of Si thickness with time has an inflection point at the moment when the roughness drops dramatically. This could represent a real phenomenon, such as a difference in deposition mode, which starts amorphous with high roughness then continues to be crystalline with smaller roughness. This could also represent a modelling artefact. This is to be confirmed and demonstrated in the future, as the failure of selectivity for certain process conditions could provide further hints to its origins.

ACKNOWLEDGMENTS

This activity is funded through the Total-LPICM ANR Industrial Chair "PISTOL" (Contract ANR-17-CHIN-0002-01). The authors acknowledge financial support from the French state managed by the National Research Agency under the Investments for the Future program (ANR-10-EQPX-50, Pole NanoTEM). The authors also acknowledge the support of the Centre Interdisciplinaire de Microscopie électronique de l'X (CIMEX).

References

- ¹ G. N. Parsons, and R. D. Clark, *Chem. Mater.* 2020, 32, 12, 4920–4953
- ² M. J. Hampden-Smith and T. T. Kodas, *Chem. Vap. Deposition* 1995. I, No, 2
- ³ A. J. M. Mackus, A. A. Bol and W. M. M. Kessels, *Nanoscale*, 2014,6, 10941-10960
- ⁴ B.D. Joyce, J.A. Baldrey, Selective epitaxial deposition of silicon, *Nature*. 195 (1962) 485–486.
- ⁵ F.W. Tausch, A.G. Lapierre, *J. Electrochem. Soc.* 112 (1965) 706.
- ⁶ J.O. Carlsson, Novel and selective vapor deposition processes, *Vacuum*. 41 (1990) 1077–1080.
- ⁷ J. Carlsson, M. Boman, *J. Vac. Sci. Technol. A Vacuum, Surfaces, Film*. 3 (1985) 2298–2302.
- ⁸ D.A. Mantell, *J. Vac. Sci. Technol. A Vacuum, Surfaces, Film*. 9 (1991) 1045–1050.
- ⁹ W.L. Gladfelter, *Chem. Mater.* 5 (1993) 1372–1388.
- ¹⁰ E. Mohimi, Z. V. Zhang, S. Liu, J. L. Mallek, G. S. Girolami, and J. R. Abelson, *J. Vac. Sci. Technol. A* 36, 041507 (2018)
- ¹¹ Z. V. Zhang, S. Liu, G. S. Girolami, and J. R. Abelson, *J. Vac. Sci. Technol. A* 38, 033401 (2020)
- ¹² T. Suh, Y. Yang, P. Zhao, K. U. Lao, H.-Y. Ko, J. Wong, R. A. DiStasio, and J. R. Engstrom, *ACS Applied Materials & Interfaces* 2020 12 (8), 9989-9999
- ¹³ D. Bobb-Semple, K. L. Nardi, N. Draeger, D. M. Hausmann, and S. F. Bent, *Chem. Mater.* 2019, 31, 1635–1645
- ¹⁴ R. Wojtecki, M. Mettry, N.F. Fine Nathel, A. Friz, A. De Silva, N. Arellano, H. Shobha, *ACS Appl. Mater. Interfaces*. 10 (2018) 38630–38637.
- ¹⁵ A. P. Hinckley, M. M. Driskill, and A. J. Muscat, *ACS Appl. Nano Mater.* 2020, 3, 3185–3194
- ¹⁶ J. Soethoudt, Y. Tomczak, B. Meynaerts, B. T. Chan, and A. Delabie, *J. Phys. Chem. C* 2020, 124, 7163–7173

- ¹⁷ T. G. Pattison, A. E. Hess, N. Arellano, N. Lanzillo, S. Nguyen, H. Bui, C. Rettner, H. Truong, A. Friz, T. Topuria, A. Fong, B. Hughes, A. T. Tek, A. DeSilva, R. D. Miller, G. G. Qiao, and R. J. Wojtecki, *ACS Nano* 2020, 14, 4276–4288
- ¹⁸ E. Stevens, Y. Tomczak, B. T. Chan, E. A. Sanchez, G. N. Parsons and A. Delabie, *Chem. Mater.* 2018, 30, 3223–3232
- ¹⁹ M. J. M. Merkx, T. E. Sandoval, D. M. Hausmann, W. M. M. Kessels, and A. J. M. Mackus, *Chem. Mater.* 2020, 32, 3335–3345
- ²⁰ R. Vallat, R. Gassilloud, B. Eychehenne, C. Vallée, *Journal of Vacuum Science & Technology A* 35, 01B104 (2017)
- ²¹ M. F. J. Vos, S. N. Chopra, M. A. Verheijen, J. G. Ekerdt, S. Agarwal, W. M. M. Kessels, and A. J. M. Mackus, *Chem. Mater.* 2019, 31, 3878–3882
- ²² G. Akiki, D. Suchet, D. Daineka, S. Filonovich, P. Bulkin, E. V. Johnson, *Applied Surface Science* 531 (2020) 147305
- ²³ H. Fujiwara, M. Kondo, and A. Matsuda, *Phys. Rev. B* 63, 115306 (2001)
- ²⁴ H. Fujiwara, M. Kondo, and A. Matsuda, *Journal of Applied Physics* 93, 2400 (2003)
- ²⁵ S. Kasouit, S. Kumar, R. Vanderhaghen, P. Roca i Cabarrocas, I. French, *J. Non. Cryst. Solids.* 299–302 (2002) 113–117
- ²⁶ J.C. Dornstetter, B. Bruneau, P. Bulkin, E. V. Johnson, P. Roca I Cabarrocas, *2014 IEEE 40th Photovolt. Spec. Conf. PVSC 2014.* (2014) 2839–2841
- ²⁷ J.F. Moulder, W.F. Stickle, P.E. Sobol, K.D. Bomben. *Handbook of X-ray photoelectron spectroscopy: a reference book of standard spectra for identification and interpretation of XPS data.* Physical Electronics: Eden Prairie, Minnesota, 1995